Polymeric Micelles for Neoadjuvant Cancer Therapy and Tumor-Primed Optical Imaging

Hyunah Cho and Glen S. Kwon*

Pharmaceutical Sciences Division, School of Pharmacy, University of Wisconsin, 777 Highland Avenue, Madison, Wisconsin 53705-2222, United States

ABSTRACT

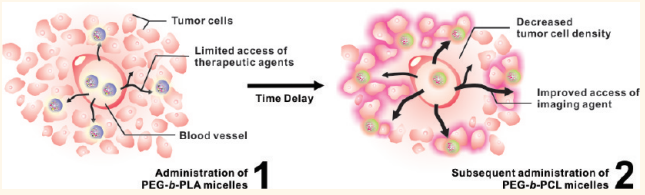

Poly(ethylene glycol)-*block*-poly(D,L-lactic acid) (PEG-*b*-PLA) micelles act as a 3-in-1 nanocontainer for three poorly water-soluble drugs—paclitaxel, 17-allylamino-17-demethoxygeldanamycin, and rapamycin (PTX/17-AAG/RAPA)—for cancer therapy. In a LS180 human colon xenograft model, a single intravenous (IV) injection of 3-in-1 PEG-*b*-PLA micelles reduced tumor volume by 1.6-fold with <10% body weight change. In a second step, IV injection of poly(ethylene glycol)-*block*-poly(ε-caprolactone) (PEG-*b*-PCL) micelles carrying a carbocyanine dye (1,1′-dioctadecyl tetramethyl indotricarbocyanine iodide (DiR)) after 48 h resulted in a 2.1-fold higher near-infrared (NIR) optical signal from excised solid tumors *versus* a negative control, presumably due to a reduction in tumor cell density and interstitial tumor pressure. Thus, a tandem of 3-in-1 PEG-*b*-PLA and PEG-*b*-PCL micelles could potentially be used for neoadjuvant cancer therapy and tumor-primed NIR optical imaging for intraoperative surgical guidance in oncology, offering a promising multimodal strategy for cancer therapy and imaging.

KEYWORDS: 17-AAG · carbocyanine dye · optical imaging · paclitaxel · polymeric micelle · rapamycin · tumor priming

Nanomaterials such as quantum dots, gold nanoparticles, and nanoparticles that contain fluorescent dyes may accumulate at solid tumors through leaky vasculature, that is, the EPR effect,[1−4] and emit fluorescence in the near-infrared (NIR) region,[5,6] raising the prospect of intraoperative surgical guidance in oncology.[7−9] While NIR optical imaging will not likely replace other imaging modalities for whole body tumor detection due to attenuation of fluorescence signals by overlying tissue, optically active nanomaterials may be used for the assessment of tumor margins, adjacent structures, and adjacent tumor deposits during surgery, supplementing visible inspection under white light and palpation.[10−12] It is noted that complete surgical resection is the single most important predictor of survival in patients with lung, breast, prostate, colon, and pancreatic cancers. However, nanomaterials for NIR optical imaging must fulfill central requirements in safety, targeted delivery,[13,14] for example, avoidance of mononuclear phagocyte system, and molecular imaging, for example, high target-to-nontarget tissue ratio.[10]

While nanomaterials will continue to evolve for NIR optical imaging and certainly merit more attention,[15,16] strategies that overcome delivery barriers in solid tumors have drawn attention in cancer nanotechnology and may be used to improve efforts in NIR optical imaging in surgical oncology. Jain has highlighted intratumoral barriers that hinder the delivery of nanomaterials into solid tumors for therapy and imaging, noting that nanomaterials >60 nm in diameter are unable to diffuse effectively in many solid tumors.[17] The distribution of blood vessels throughout solid tumors is uneven; simply, tumor regions lacking blood vessels will receive less nanomaterial than regions perfused with plenty of blood vessels.[18−22] Solid tumors have high interstitial fluid pressure that diminishes the penetration of nanomaterials from blood vessels into tumors by convection.[22] To overcome delivery barriers at solid tumors, strategies such as co-injection of enzymes that degrade the extracellular matrix have been researched. Jain proposed the vascular normalization hypothesis for enhanced intratumoral drug delivery, although its relevance for nanomaterial is less clear.[17] Au and co-workers proposed a strategy, termed "tumor priming," where pretreatment with the single intravenous (IV) injection of a potent anticancer drug such as paclitaxel (PTX) results in tumor cell apoptosis, reduction in tumor cell density, and expansion of interstitial space.

* Address correspondence to gskwon@pharmacy.wisc.edu.

Received for review July 16, 2011 and accepted October 15, 2011.

Published online October 16, 2011
10.1021/nn202676u

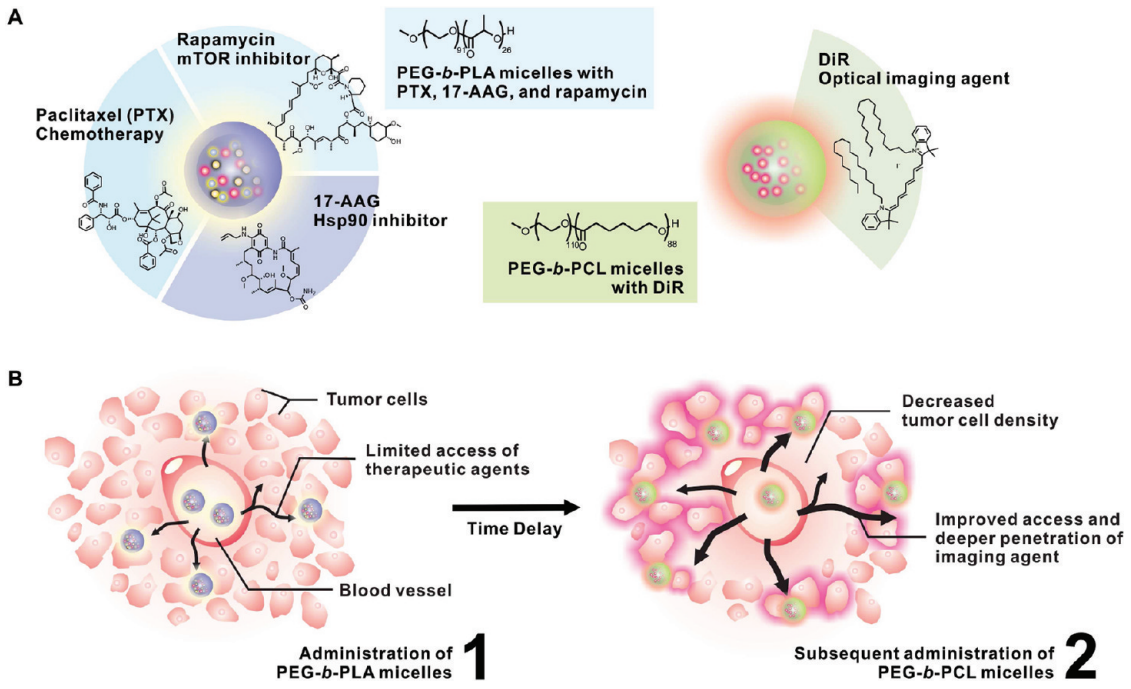

Figure 1. (A) The 3-in-1 PEG-*b*-PLA micelles containing PTX/17-AAG/RAPA with the *z*-average diameter of 37.5 ± 0.74 (PDI: 0.125 ± 0.021) and drug loading capacity of 40.4 ± 1.2% (drugs/polymer), and PEG-*b*-PCL micelles containing DiR with the *z*-average diameter of 47.05 ± 1.80 (PDI: 0.154 ± 0.017) and DiR loading capacity of 2.30 ± 0.20% (DiR/polymer). (B) Schematic illustration of tumor-primed delivery of NIR optical imaging agent (DiR) by a tandem of PEG-*b*-PLA and PEG-*b*-PCL micelles.

As a result, liposomes that contain doxorubicin had higher uptake at solid tumors. It is noted that tumor priming was selective for the solid tumors even though the standard formulation of PTX (40 mg/kg) that contains Cremophor EL was used (Taxol).[19,20] Regardless of the proposed strategy for overcoming barriers of nanomaterial uptake into solid tumors, it must be done safely, selectively for solid tumors, and can be achieved after systemic administration, preferably by IV injection or infusion.[23]

Polymeric micelles are a major class of nanomaterials that have entered several clinical trials for drug delivery,[23,24] and they have drawn recent attention for optical imaging. Herein, we propose a tandem of polymeric micelles for a combined drug delivery and optical imaging strategy, aiming for tumor debulking, tumor priming, and enhanced NIR optical imaging of solid tumors (Figure 1). Poly(ethylene glycol)-*block*-poly(D,L-lactic acid) (PEG-*b*-PLA) micelles act as a nanocontainer for two or three poorly water-soluble anticancer drugs, enabling concurrent IV administration of multiple anticancer drugs for the first time.[25] PEG-*b*-PLA micelles will replace organic cosolvents and toxic surfactants, for example, Cremophor EL, that are required for drug solubilization for the IV route, noting that PEG-*b*-PLA micelles carrying PTX (Genexol-PM) are approved in several Asian countries for cancer therapy and are in phase III clinical trials in the USA.[26,27] In our recent work, PEG-*b*-PLA micelles act as a 3-in-1 nanocontainer for PTX, 17-allylamino-17-demethoxygeldanamycin, and rapamycin (PTX/17-AAG/RAPA), and we hypothesize that 3-in-1 PEG-*b*-PLA micelles can be used for neoadjuvant cancer therapy and for tumor priming for NIR optical imaging (Figure 1).[28] For tumor priming, PEG-*b*-PLA is much less toxic than Cremophor EL in Taxol, noting a 2-fold higher maximum tolerated dose (MTD) for PTX in clinical trials for Genexol-PM. The 2- and 3-drug combinations of PTX, 17-AAG, and RAPA exert synergistic cytotoxicity toward breast, lung, ovarian, and colon cell lines (data not shown). After tail vein injections of 3-in-1 PEG-*b*-PLA micelles with PTX/17-AAG/RAPA at 60, 60, and 30 mg/kg on days 0, 4, and 8, there was <10% body weight change and no deaths, noting that the MTD in nude mice for Genexol-PM is 60 mg/kg on the same dosing schedule and the MTD for Taxol is 20 mg/kg.[28]

For NIR optical imaging, poly(ethylene glycol)-*block*-poly(ε-caprolactone) (PEG-*b*-PCL) micelles act as long-circulating nanomaterials that accumulate preferentially at solid tumors *via* the EPR effect (Figure 1). Allen and co-workers nonevasively monitored the fate of ^{111}In-labeled PEG-*b*-PCL micelles by microSPECT/CT imaging and showed that they have prolonged circulation in blood and preferential localization at solid tumors (9.0 ± 2% dose/g) in a MDA-MB-231-human breast xenograft model.[29] In our recent work, we have shown that PEG-*b*-PCL micelles have a high capacity for a lipophilic carbocyanine dye, DiR (1,1′-dioctadecyl tetramethyl indotricarbocyanine iodide), a carbocyanine dye that has strong light absorbance in the NIR region (700−800 nm), rendering deep-tissue penetration of light with low autofluorescence.[30] In a LS180

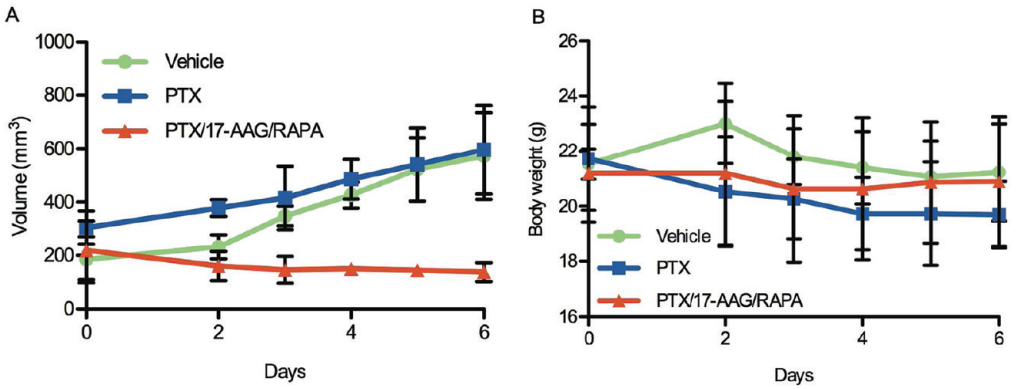

Figure 2. Effects of PEG-*b*-PLA micelles carrying PTX/17-AAG/RAPA, PTX, or vehicle control on (A) tumor growth and (B) body weight (mean ± SD; *n* = 3/treatment group).

human colon xenograft model, PEG-*b*-PCL micelles carrying DiR preferentially illuminated solid tumors, having tumor-to-muscle ratios of 30−43, depending on the aggregation state of DiR in PEG-*b*-PCL micelles. In this work, we show how a tandem of 3-in-1 PEG-*b*-PLA and PEG-*b*-PCL micelles carrying DiR can be used for tumor debulking, tumor priming, and enhanced NIR optical imaging of solid tumors in a LS180 human colon xenograft model, coupling progress in drug delivery and NIR optical imaging for advances in integrated cancer therapy involving nanomedicine and surgical oncology.

RESULTS AND DISCUSSION

Antitumor Activity of 3-in-1 PEG-*b*-PLA Micelles. After solid tumors reached 200−300 mm^3 in a LS180 human colon xenograft model, 3-in-1 PEG-*b*-PLA micelles carrying PTX/17-AAG/RAPA (60/60/30 mg/kg), PEG-*b*-PLA micelles carrying PTX (60 mg/kg), or empy PEG-*b*-PLA micelles as a vehicle control were injected intravenously, and tumor volume and body weight were measured daily for 6 days (Figure 2A). In the vehicle control, tumors gradually increased over 6 days, reaching *ca.* 580 mm^3. Similarly, tumors gradually increased over 6 days in the same way for PEG-*b*-PLA micelles carrying PTX, although at day 2 tumor volume for PTX appeared slightly smaller than the vehicle control. In contrast, a single IV injection of 3-in-1 PEG-*b*-PLA micelles reduced tumor volume by 1.6-fold, reaching *ca.* 100 mm^3. At the same time, body weights of mice treated with 3-in-1 PEG-*b*-PLA micelles declined slightly, but the decrease was <10% with no deaths, suggesting acceptable acute toxicity (Figure 2B). Similar acute toxicity results were observed for the vehicle control and PEG-*b*-PLA micelles carrying PTX at 60 mg/kg. Other options for concurrent and sequential deliveries of three drugs are injecting a mixture of three individual single drug-loaded micelles (3-in-3 micelles) and separately injecting the 3 corresponding micelles (3 × 1-in-1 micelles), repectively. However, the strategy of using 3-in-1 micelles would be more practical by minimizing injection volume compared to IV injections of 3 individual single drug-loaded micelles as the minimum injection volume for either 3-in-3 or 3 × 1-in-1 micelles would be beyond the volume limit for IV administration to mice (blood volume 1.2−1.6 mL). In summary, 3-in-1 PEG-*b*-PLA micelles exerted potent antitumor efficacy after a single IV injection, whereas PEG-*b*-PLA micelles carrying PTX at 60 mg/kg was no different than the vehicle control. These *in vivo* results were at odds with *in vitro* cell culture experiments, which showed that PTX is at least as potent as PTX/17-AAG/RAPA in terms of IC_{50} value (*ca.* 170 nM) against LS180 human colon cells (data not shown), whereas 17-AAG and RAPA were ineffective (>10 000 nM). We speculate that 17-AAG, a heat shock protein 90 (Hsp90) inhibitor, and RAPA, a mammalian target of rapamycin (mTOR), inhibitor act in concert with PTX on both tumor cells and tumor-associated stromal cells, whereas PTX acts primarily on tumor cells, limiting its antitumor response in an *in vivo* setting.

Whole-Body NIR Optical Imaging. In a FaDu human hypopharyngeal carcinoma xenograft model, PTX as Taxol injected IV at 40 mg/kg caused maximum apoptosis at solid tumors (>10%) after 2 to 3 days.[19] For NIR optical imaging of solid tumors, PEG-*b*-PCL micelles carrying DiR (230 μg/kg) were injected intravenously 2 days after the primary IV injection of 3-in-1 PEG-*b*-PLA micelles carrying PTX/17-AAG/RAPA (60/60/30 mg/kg), PEG-*b*-PLA micelles carrying PTX (60 mg/kg), or empy PEG-*b*-PLA micelles. PEG-*b*-PCL micelles carrying DiR clearly delineated solid tumors based on whole-body optical imaging of DiR at 800 nm (Figure 3). The optical signal of DiR at solid tumors in mice clearly overlapped with solid tumors observed under white light. In all three test cases, the fluorescence signal intensity of DiR at solid tumors increased over 24 h and had a high average radiant efficiency at in the region of interest (ROI), that is, the tumor (*ca.* 5 × 10^9 [p/s/cm^2/sr]/[μW/cm^2]), and high ratio of average radiant efficient at the ROI relative to whole body (*ca.* 6 at 24 h). The ROI-to-whole body ratios for DiR were not statistically different

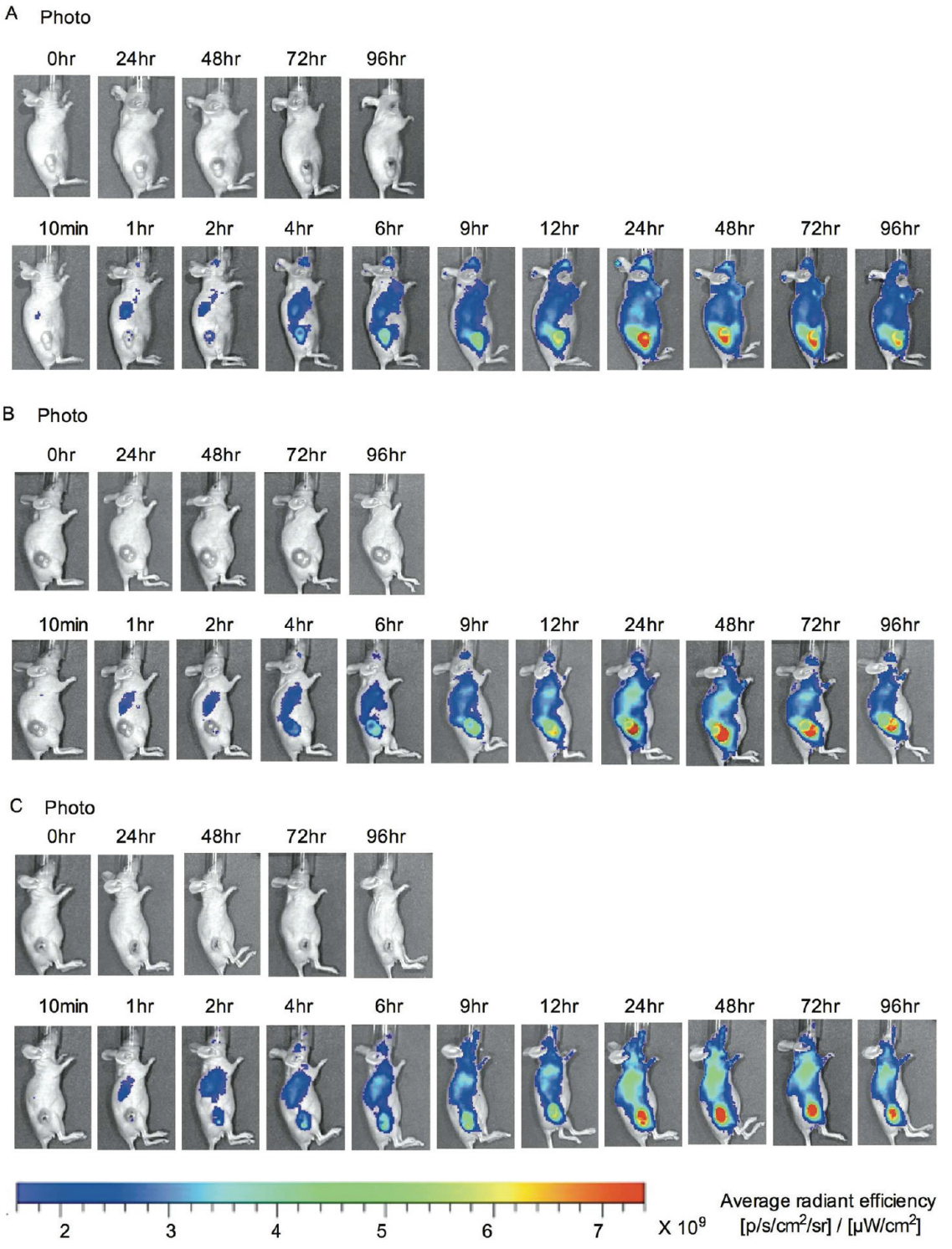

Figure 3. Whole-body NIR optical imaging of DiR. (A) Empty PEG-*b*-PLA micelles (vehicle), (B) PTX, or (C) PTX/17-AAG/RAPA were injected IV 48 h before the injection of DiR-containing PEG-*b*-PCL micelles.

for the three test cases (data not shown). In summary, whole-body NIR imaging of DiR in PEG-*b*-PCL micelles after IV injection showed preferential accumulation of DiR at solid tumors in a LS180 human colon xenograft model due to the EPR effect, owing to PEG-*b*-PCL micelles. However, whole-body NIR imaging was unable to distinguish tumor priming effects of 3-in-1 PEG-*b*-PLA micelles, although an obvious antitumor response was observed (Figures 2 and 3). We suspected that actual differences in fluorescence intensity of DiR of subcutaneously inoculated tumors were blurred under superficial skin layers, and we turned to *ex vivo* NIR optical imaging as a better surrogate of intraoperative NIR surgical guidance for tumor resection and to better

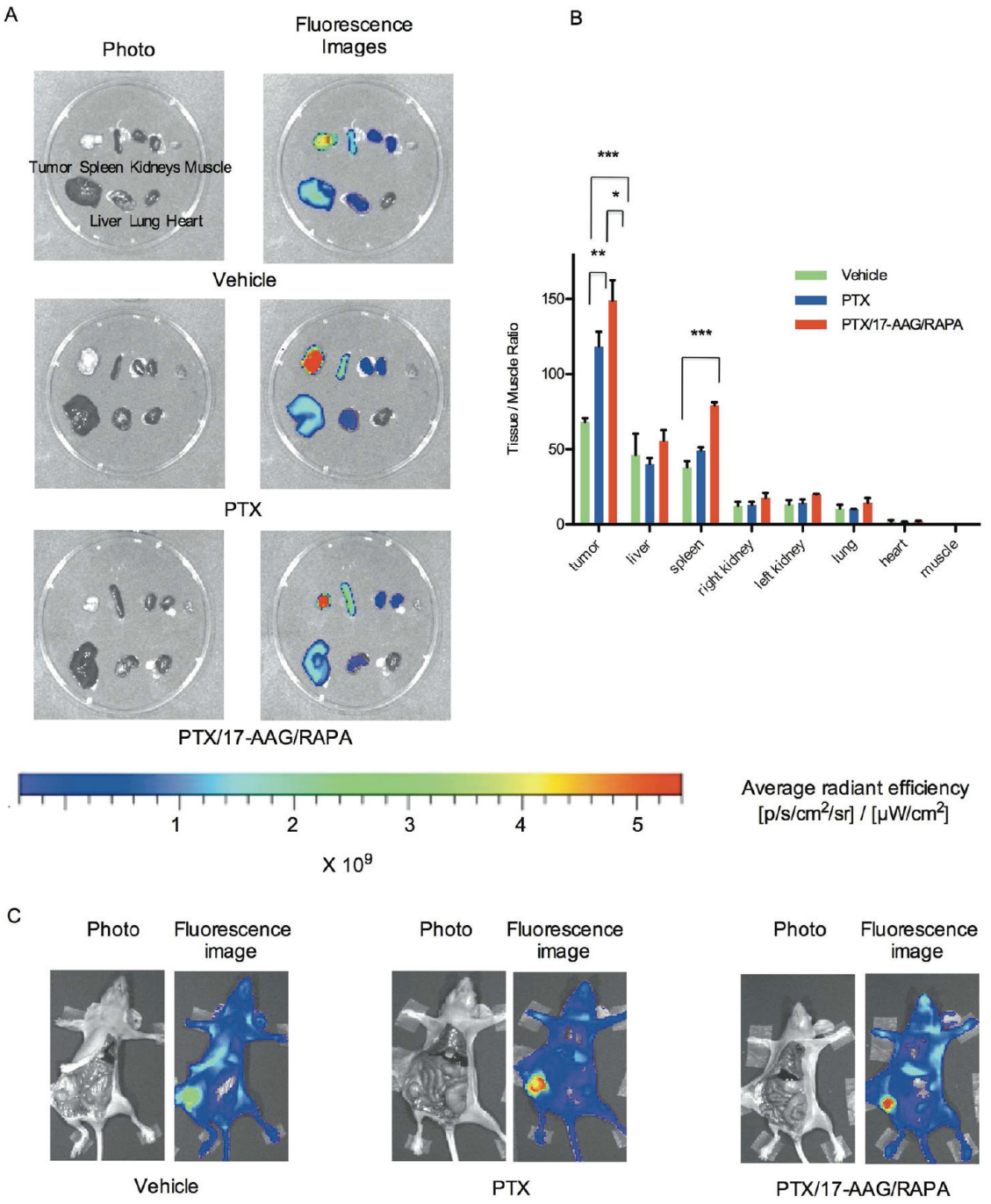

Figure 4. (A,B) *Ex vivo* NIR optical imaging of DiR after treatment with empty PEG-*b*-PLA micelles (vehicle), PTX, or PTX/17-AAG/RAPA, injected IV 48 h before the injection of DiR-containing PEG-*b*-PCL micelles (mean ± SD; *n* = 3/treatment group; (∗) <0.05, (∗∗) <0.01, (∗∗∗) <0.0001). (C) Whole-body NIR optical images of DiR (solid tumors in the right flank) after a midline incision in the abdomen.

ascertain the feasibility of 3-in-1 PEG-*b*-PLA micelles for tumor-primed NIR optical imaging.

***Ex Vivo* NIR Optical Imaging.** After 4 days of whole-body NIR optical imaging (6 days post-primary injection), mice were sacrificed by CO_2 asphxia, and organs and tissues were surgically resected and subjected to *ex vivo* NIR optical imaging (Figure 4). Optical images of dissected tumors showed the highest level of fluorescence signal intensity of DiR, followed by the liver and spleen. Kidneys, lungs, heart, and muscle had low fluorescence signal intensity for DiR, indicating a limited volume of distribution for DiR. In the color-coded fluorescence images of tumor tissue, noticeable differences between the three test cases were discerned: mice treated with a primary IV injection of 3-in-1 PEG-*b*-PLA micelles carrying PTX/17-AAG/RAPA displayed a red color, whereas mice treated with a vehicle control displayed a yellow color, *ca.* 1.3-fold reduction in

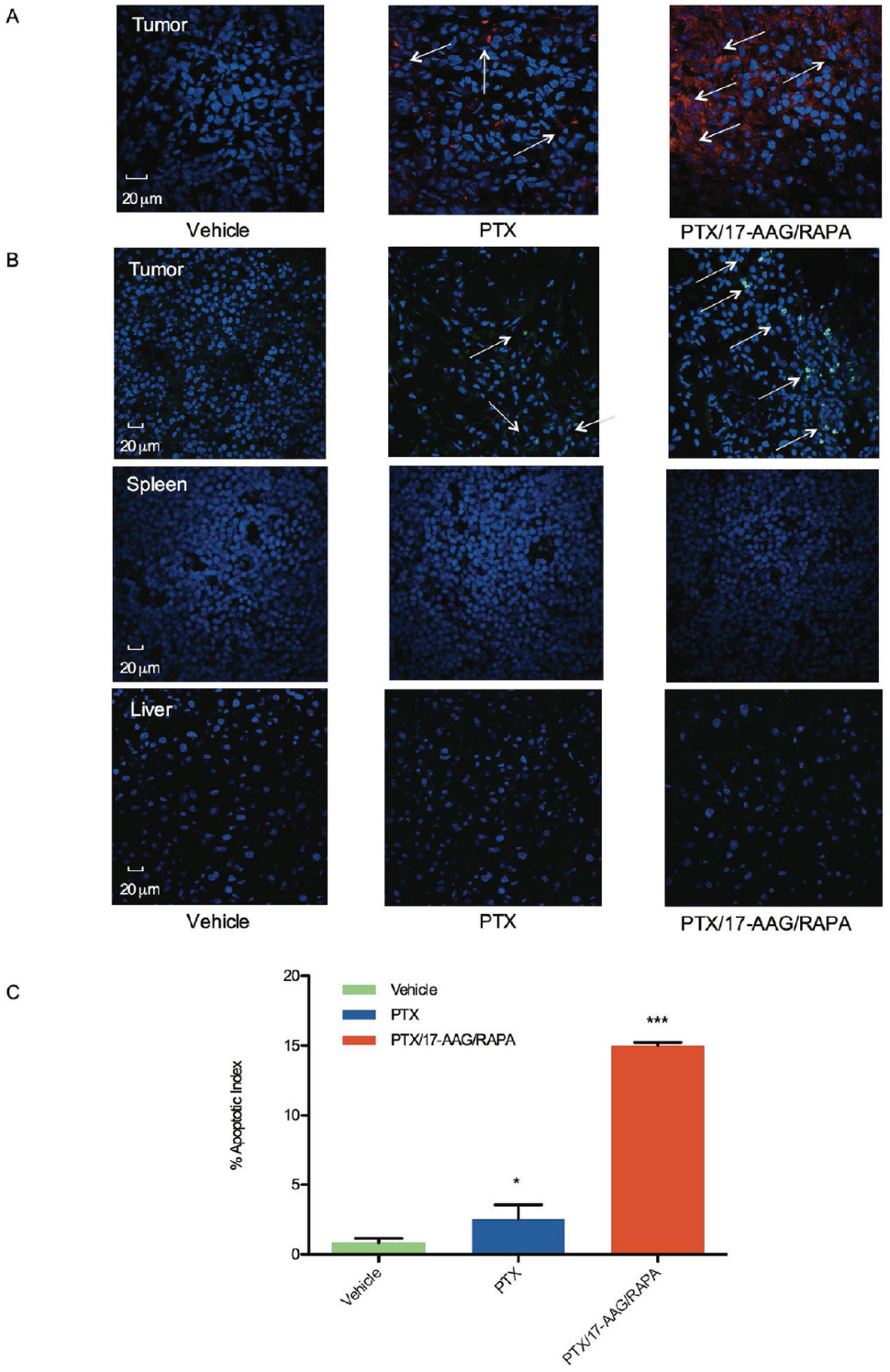

Figure 5. (A) Laser scanning confocal microscopy images of tumor tissue (60× magnification). DiR is red, and nuclei of cells are in blue (DAPI). (B) Immunohistochemical analysis of apoptosis by TUNEL in tumor, spleen, and liver tissues (40× magnification). Apoptotic cells are in green, and nuclei of all cells are in blue (DAPI). (C) Apoptosis index (mean ± SD; *n* = 3/treatment group; (∗) <0.05, (∗∗∗) <0.0001).

fluorescence signal intensity (Figure 4). Tumor-to-muscle ratios are often used as a gauge of tumor selectivity in the evaluation of nanomaterials and were calculated for DiR based on *ex vivo* optical imaging (Figure 4B). The tumor-to-muscle ratio for mice treated with 3-in-1 PEG-*b*-PLA micelles carrying PTX/17-AAG/RAPA was 149 ± 13, whereas the value for mice treated with PEG-*b*-PLA micelles carrying PTX was 118 ± 10. The tumor-to-muscle ratio for vehicle control was 68 ± 3. Thus, *ex vivo* NIR optical imaging revealed a 2.1- and

1.7-fold increase for the 2 pretreatment groups, respectively, suggestive of higher tumor levels of DiR. Notably, increases in tumor-to-muscle ratios for DiR were not accompanied by statistically higher values for other organs with the exception of the spleen for 3-in-1 PEG-*b*-PLA micelles (Figure 4B), suggesting selectivity in tumor priming for NIR optical imaging. Additional evidence for the enhanced uptake of DiR at solid tumors was obtained from resected tumor tissue, which was collected, fixed with 4% paraformaldehyde, sectioned into 10 μm slices, and visualized by laser scanning confocal microscopy (Figure 5A). In this study, DiR was readily observed as red dots in resected tumors for mice pretreated with 3-in-1 PEG-*b*-PLA micelles. A few red dots were also observed for the PTX group, whereas there were faint signs of DiR for the vehicle control. One limitation of this study was the use of a laser filter set at 635 nm, which is nonoptimal for DiR. Still, these qualitative results from resected tumor tissue support the *ex vivo* NIR optical results, which suggest an enhanced tumor accumulation of DiR, particularly after tumor priming with 3-in-1 PEG-*b*-PLA micelles. Finally, apoptosis at solid tumors, spleen, and liver was assessed by the Tdt-mediated dUTP NickEnd Labeling (TUNEL) method (Figure 5B). Apoptotic cells (in green) were clearly visible in solid tumors with 3-in-1 PEG-*b*-PLA micelles. Importantly, apoptotic cells were not visible at the liver and spleen. In this study, the apoptotic index, that is, apoptotic bodies in an area having 100 nuclei (stained in blue), was 15 $\pm$ 0.22 for 3-in-1 PEG-*b*-PLA micelles and 3 $\pm$ 1.02 for the PTX group. It was quite remarkable that apoptosis at solid tumors was evident after 6 days following a single IV injection of 3-in-1 PEG-*b*-PLA micelles, but is consistent with the reduction in tumor volume at day 6, *ca.* 100 mm^3 *versus* 580 mm^3 for the PTX group (Figure 2).

While the mechanisms behind the enhanced uptake of DiR and high NIR optical signal at solid tumors remain to be fully elucidated, tumor-associated apoptosis was evident and clearly a factor in tumor priming. Au and co-workers proposed that PTX as Taxol-injected IV at 40 mg/kg reduced tumor cell density, expanded microvessel diameter, and promoted tumor perfusion.[19] It is noted that tumor priming with PTX as Taxol in a FaDu human hypopharyngeal carcinoma xenograft model was tumor-selective, resulting in enhanced accumulation of liposomes that contain doxorubicin at solid tumors, but not at other organs, consistent with our *ex vivo* NIR optical imaging results on DiR, delivered by PEG-*b*-PCL micelles. Other possible mechanisms behind the enhanced uptake of DiR and high NIR optical signal at solid tumors may also include reduced interstitial tumor fluid pressure and vascular normalization as proposed by Jain, noting that PTX, 17-AAG, and RAPA all have antiangiogenesis activity.

CONCLUSIONS

NIR optical imaging has unique potential for intraoperative surgical guidance in oncology, beyond simple visualization with white light illumination, palpation, and experience, which is a major factor in surgical oncology. In a LS180 human colon xenograft model, 3-in-1 PEG-*b*-PLA micelles carrying PTX/17-AAG/RAPA induced apoptosis at solid tumors and illicited a striking 1.6-fold reduction in tumor volume after a single IV injection with low acute toxicity. Hence, 3-in-1 PEG-*b*-PLA micelles promoted the delivery PEG-*b*-PCL micelles carrying DiR into solid tumors, resulting in heightened NIR optical signal for better tumor delineation. This "priming effect" was largely selective for solid tumors, achieving a remarkable tumor-to-muscle ratio of 149 $\pm$ 13 for DiR in resected tissue. Thus, a tandem of 3-in-1 PEG-*b*-PLA and PEG-*b*-PCL micelles carrying DiR was used for effective tumor debulking, heightened tumor priming, and enhanced NIR optical imaging of solid tumors. It is noted that neoadjuvant therapy is commonly used for the debulking of solid tumor prior to surgical procedures. Future research will assess the potential of 3-in-1 PEG-*b*-PLA and PEG-*b*-PCL micelles for intraoperative surgical guidance in human xenograft models, assessing neoadjuvancy and NIR optically guided surgery on the effectiveness of surgical resection of tumors and ultimately survival. Beyond enhanced NIR optical imaging of solid tumors, tumor priming by 3-in-1 PEG-*b*-PLA micelles carrying PTX/17-AAG/RAPA merits consideration for the tumor targeting of nanomedicines in multimodal interventions in cancer therapy.

MATERIALS AND METHODS

Preparation and Characterization of 3-in-1 PEG-*b*-PLA Micelles and PEG-*b*-PCL Micelles Carrying DiR. The methods used to prepare PEG-*b*-PLA and PEG-*b*-PCL micelles have been described elsewhere.[29] Briefly, 15 mg of PEG-*b*-PLA at M_n of PEG = 4 200 g/mol; M_n of PLA = 1 900 g/mol; and M_w/M_n = 1.06 (Advanced Polymer Materials Inc., Montreal, Canada) and 2.0 mg of PTX, 2.0 mg of 17-AAG, and 1.5 mg of RAPA (LC Laboratories, Woburn, MA) were dissolved in 0.5 mL of acetonitrile in a round-bottom flask, followed by solvent evaporation under reduced pressure using a rotatory evaporator at 60 °C until a thin, even film was formed. The polymeric film was rehydrated with 0.5 mL of double-distilled H_2O or 0.9% saline. The aqueous solution was centrifuged for 5 min at 10 000 *g* to remove water insoluble drugs and passed through 0.45 μm nylon syringe filter (National Scientific, Rockwood, TN).

PEG-*b*-PCL micelles were prepared by a distinct method: 4.0 mg of PEG-*b*-PCL at M_n = 5 000 g/mol; M_n of PCL = 10 000 g/mol; and M_w/M_n = 1.3 (Polymer Source, Dorval, Canada) and 0.10 mg of DiR (Caliper Life Science, Hopkinton, MA) were dissolved in 2.0 mL of acetone, followed by a rapid addition of 2.0 mL of double-distilled H_2O or 0.9% saline with vigorous mixing. Acetone was allowed to evaporate from the aqueous micelle solution under stirring at room temperature for 40 min.

The aqueous micelle solution was centrifuged for 5 min at 10 000 *g* to remove insoluble DiR and passed through 0.45 μm nylon syringe filter.

The content of PTX, 17-AAG, and RAPA in PEG-*b*-PLA micelles and content of DiR in PEG-*b*-PCL micelles was quantified by reverse-phase HPLC analysis, using a Shimadzu Prominence HPLC system (Shimadzu, Japan) equipped with an LC-20AT pump, a SIL-20AC HT autosampler, a CTO-20AV oven, and an SPD-M20A diode array detector. Aqueous micelle solutions (10 μL) were injected into a Zorbax SB-C8 Rapid Resolution cartridge (4.6 mm $\times$ 75 mm, 3.5 μm, Agilent). The flow rate was 1.0 mL/min, and column temperature was kept at 40 °C. The separation of PTX, 17-AAG, and RAPA was done in isocratic mode with mobile phase consisting of 55% acetonitrile and 45% double-distilled H_2O containing 0.1% phosphoric acid and 1% methanol. PTX, 17-AAG, and RAPA were monitored at 227, 333, and 279 nm and eluted at 2.8, 3.3, and 8.6 min, respectively. The elution of DiR was done in a gradient mode with the mobile phase consisting of 30% acetonitrile containing 0.03% trifluoroacetic acid as solvent A and 70% double-distilled H_2O containing 0.07% trifluoroacetic acid as solvent B. Gradient elution was employed according to the following linear program: 0 min, 100% solvent A and 0% solvent B; 32 min, 30% solvent A and 70% solvent B. DiR was monitored at 745 nm and eluted at 16 min.

z-Average diameters of 3-in-1 PEG-*b*-PLA micelles and PEG-*b*-PCL micelles carrying DiR were determined by dynamic light scattering measurement using a Zetasizer Nano-ZS (Malvern Instruments, UK) at 25 °C with a detection angle of 173° and a He−Ne ion laser (λ = 633 nm) for the incident beam. The correlation function was curve-fitted by the cumulant method, and the *z*-average diameters of PEG-*b*-PLA and PEG-*b*-PCL micelles were obtained by single exponential algorithm. All measurements were repeated three times, and the *z*-average diameter was presented as an average plus or minus standard deviation. The width of the distribution was estimated by the polydispersity index.

LS180 Human Colon Xenograft Model. LS180 human colon carcinoma cells were cultivated in minimum essential medium including Earle's salts (Cellgro, Manassas, VA), supplemented with 2% sodium bicarbonate, 1% nonessential amino acids, 1% sodium pyruvate, 10% fetal bovine serum, 1% L-glutamine, and 100 U/mL penicillin−streptomycin solution. Cells were maintained at 37 °C under an atmosphere of 5% CO_2 in a humidified incubator. Cells with >90% viability were harvested from subconfluent cultures after trypsinization, and 1×10^6 cells were inoculated subcutaneously into the right flank of anesthetized female 6−8 week-old nude mice (Laboratory Animal Resources, Madison, WI). General anesthesia was induced with 1.5% isoflurane/oxygen, and anesthesia was maintained with 1% isoflurane/oxygen. When solid tumors reached 200−300 mm^3, mice were randomly divided into three groups (n = 3): 3-in-1 PEG-*b*-PLA micelles with PTX, 17-AAG, and RAPA at 60, 60, and 30 mg/kg, PEG-*b*-PLA micelles with PTX at 60 mg/kg; and empty PEG-*b*-PLA micelles as a control. Each treatment group was injected through the tail vein of anesthetized animals. Thereafter, tumor volumes and body weights were measured by a digital caliper (Fisher Scientific, Pittsburgh, PA) and a portable scale everyday for 6 days. In the mean time, the behavior of animals was monitored. All animal experiments were approved by UW-Madison's institutional animal care and use committee.

Whole-Body NIR Optical Imaging. Two days after the primary injection of PEG-*b*-PLA micelles, PEG-*b*-PCL micelles carrying DiR (230 μg/kg) were injected through the tail vein of anesthetized animals. Whole-body images were recorded at 10 min and at 1, 2, 4, 6, 9, 12, 24, 48, 72, and 96 h, using Xenogen IVIS 200 series (Caliper Life Sciences, Hopkinton, MA). Mice were placed in lateral positions to obtain whole-body optical images color-coded by the fluorescence of DiR, with the filter set at excitation and emission wavelengths of 745 and 800 nm, respectively. In this time course experiment, all images were collected using identical system settings, and the fluorescence emission of DiR was normalized by average radiant efficiency, total photons per second per square centimeter per steradian in the irradiance range (microwatts per square centimeter): [p/s/cm^2/sr]/[μW/cm^2]), using Living Imaging software. For comparison, a region of interest (ROI) was outlined around the solid tumor region, and the fluorescence intensity of DiR associated with the tumor was measured. The tumor-to-whole body fluorescence intensity ratio for DiR was calculated to evaluate the selective accumulation of DiR incorporated in PEG-*b*-PCL micelles at solid tumors.

***Ex Vivo* NIR Optical Imaging.** After 4 days of whole-body NIR optical imaging (6 days post-primary injection), all animals were sacrificed by CO_2 asphyxia. A surgical midline incision was done with sterilized microsurgical instruments, and the abdomen of animals was opened to simulate surgical tumor resection. Tumor, liver, lung, heart, spleen, kidneys, and muscle tissues were excised and rinsed. ROIs were drawn around the tissues, and the tissue-to-muscle ratios were calculated to evaluate relative tissue accumulation of DiR.

Laser Scanning Confocal Microscopy. Freshly isolated tissues were fixed with 4% paraformaldehyde in PBS at 4 °C and immersed in 30% sucrose in PBS solution for 1 h. Tissue blocks were embedded and completely covered by Tissue-Tek OCT compound (Sakura Finetek, Japan) in intermediate specimen cryomold (Sakura Finetek, Japan), and stored at −80 °C. Sections (10 μm-thick) were prepared using a cryotome cryostat and placed on superfrost microscope slides (Fisher Scientific, Pittsburgh, PA). A drop of mounting media (Thermo Fischer Scientific, Fremont, CA) was added on sections before placing a glass coverslip (Fisher Scientific, Pittsburgh, PA) on the slides. The nuclei of cells were stained by DAPI (Invitrogen, Carlsbad, CA). DAPI and DiR were visualized at 460 and 635 nm, respectively, using a laser scanning confocal microscope (Olympus FV1000 FLUOVIEW, Minneapolis, MN). A sampling of 20 tumor sections among 100 tumor sections was randomly selected and each tumor was marked by different colored-tapes in each group. The operator who did not have knowledge of the identity of the slides conducted a blind observation.

TUNEL Assay. DNA fragmentation resulting from apoptosis in tumor, spleen, and liver tissues was detected by the TdT-mediated dUTP Nick-End Labeling method (TUNEL) using a DeadEnd Fluorometric TUNEL assay kit (Promega, Madison, WI). Frozen tissue sections were permeabilized by proteinase K and fixed with 4% formaldehyde in PBS solution. The reaction mixture containing TdT, and fluorescein-labeled dUTP was added to sectioned tissue and incubated for 60 min at 37 °C in the humidified chamber under the dark condition. Nuclei of cells were counterstained with DAPI. Fluorescein-labeled DNA fragments were visualized at 520 nm, and blue-colored nuclei stained by DAPI were visualized at 460 nm by using a laser scanning confocal microscope (Olympus FV1000 FLUOVIEW, Minneapolis, MN). The apoptotic index was determined as the number of green-colored DNA fragments (apoptotic cells) in the area showing 100 blue-colored nuclei. This study was also conducted by blind observation.

Statistical Analysis. Statistical analysis was performed using one-way ANOVA at 5% significance level combined with Tukey's multiple comparison tests provided by GraphPad Prism version 5.00 for Mac OS X (San Diego, CA).

REFERENCES AND NOTES

1. Farokhzad, O. C.; Langer, R. Impact of Nanotechnology on Drug Delivery. *ACS Nano* **2009**, *3*, 16–20.
2. Rao, J. Shedding Light on Tumors Using Nanoparticles. *ACS Nano* **2008**, *2*, 1984–1986.
3. Hammond, P. T. Virtual Issue on Nanomaterials for Drug Delivery. *ACS Nano* **2011**, *5*, 681–684.
4. Hori, K.; Nishihara, M.; Yokoyama, M. Vital Microscopic Analysis of Polymeric Micelle Extravasation from Tumor Vessels: Macromolecular Delivery According to Tumor Vascular Growth Stage. *J. Pharm. Sci.* **2010**, *99*, 549–562.
5. He, X.; Wang, K.; Cheng, Z. *In Vivo* Near-Infrared Fluorescence Imaging of Cancer with Nanoparticle-Based Probes. *Wiley Interdiscip. Rev. Nanomed. Nanobiotechnol.* **2010**, *2*, 349–366.
6. Tian, Y.; Wu, W. C.; Chen, C. Y.; Jang, S. H.; Zhang, M.; Strovas, T.; Anderson, J.; Cookson, B.; Li, Y.; Meldrum, D.; et al. Utilization of Micelles Formed from Poly(ethylene glycol)-*block*-poly(epsilon-caprolactone) Block Copolymers as

Nanocarriers to Enable Hydrophobic Red Two-Photon Absorbing Emitters for Cells Imaging. *J. Biomed. Mater. Res. A.* **2010**, *93*, 1068–1079.
7. Kim, T. H.; Chen, Y.; Mount, C. W.; Gombotz, W. R.; Li, X.; Pun, S. H. Evaluation of Temperature-Sensitive, Indocyanine Green-Encapsulating Micelles for Noninvasive Near-Infrared Tumor Imaging. *Pharm. Res.* **2010**, *27*, 1900–1913.
8. Altinoglu, E. I.; Russin, T. J.; Kaiser, J. M.; Barth, B. M.; Eklund, P. C.; Kester, M.; Adair, J. H. Near-Infrared Emitting Fluorophore-Doped Calcium Phosphate Nanoparticles for *in Vivo* Imaging of Human Breast Cancer. *ACS Nano* **2008**, *2*, 2075–2084.
9. Singhal, S.; Nie, S.; Wang, M. D. Nanotechnology Applications in Surgical Oncology. *Annu. Rev. Med.* **2010**, *61*, 359–373.
10. Frangioni, J. V. *In Vivo* Near-Infrared Fluorescence Imaging. *Curr. Opin. Chem. Biol.* **2003**, *7*, 626–634.
11. Keramidas, M.; Josserand, V.; Righini, C. A.; Wenk, C.; Faure, C.; Coll, J. L. Intraoperative Near-Infrared Image-Guided Surgery for Peritoneal Carcinomatosis in a Preclinical Experimental Model. *Br. J. Surg.* **2010**, *97*, 737–743.
12. Mieog, J. S.; Hutteman, M.; Van der Vorst, J. R.; Kuppen, P. J.; Que, I.; Dijkstra, J.; Kaijzel, E. L.; Prins, F.; Lowik, C. W.; Smit, V. T.; Vahrmeijer, A. L.; et al. Image-Guided Tumor Resection Using Real-Time Near-Infrared Fluorescence in a Syngeneic Rat Model of Primary Breast Cancer. *Breast Cancer Res. Treat.* **2010**, *128*, 679–689.
13. Lee, H.; Hoang, B.; Fonge, H.; Reilly, R. M.; Allen, C. *In Vivo* Distribution of Polymeric Nanoparticles at the Whole-body, Tumor, and Cellular Levels. *Pharm. Res.* **2010**, *27*, 2343–2355.
14. Lee, H.; Fonge, H.; Hoang, B.; Reilly, R. M.; Allen, C. The Effects of Particle Size and Molecular Targeting on the Intratumoral and Subcellular Distribution of Polymeric Nanoparticles. *Mol. Pharm.* **2010**, *7*, 1195–1208.
15. Texier, I.; Goutayer, M.; Da Silva, A.; Guyon, L.; Djaker, N.; Josserand, V.; Neumann, E.; Bibette, J.; Vinet, F. Cyanine-Loaded Lipid Nanoparticles for Improved *in Vivo* Fluorescence Imaging. *J. Biomed. Opt.* **2009**, *14*, 054005.
16. Kalchenko, V.; Shivtiel, S.; Malina, V.; Lapid, K.; Haramati, S.; Lapidot, T.; Brill, A.; Harmelin, A. Use of Lipophilic Near-Infrared Dye in Whole-Body Optical Imaging of Hematopoietic Cell Homing. *J. Biomed. Opt.* **2006**, *11*, 050507.
17. Jain, R. K.; Stylianopoulos, T. Delivering Nanomedicine to Solid Tumors. *Nat. Rev. Clin. Oncol.* **2010**, *7*, 653–664.
18. Tredan, O.; Galmarini, C. M.; Patel, K.; Tannock, I. F. Drug Resistance and the Solid Tumor Microenvironment. *J. Natl. Cancer Inst.* **2007**, *99*, 1441–1454.
19. Lu, D.; Wientjes, M. G.; Lu, Z.; Au, J. L. Tumor Priming Enhances Delivery and Efficacy of Nanomedicines. *J. Pharmacol. Exp. Ther.* **2007**, *322*, 80–88.
20. Au, J. L.; Jang, S. H.; Zheng, J.; Chen, C. T.; Song, S.; Hu, L.; Wientjes, M. G. Determinants of Drug Delivery and Transport to Solid Tumors. *J. Controlled Release* **2001**, *74*, 31–46.
21. Jang, S. H.; Wientjes, M. G.; Lu, D.; Au, J. L. Drug Delivery and Transport to Solid Tumors. *Pharm. Res.* **2003**, *20*, 1337–1350.
22. Stohrer, M.; Boucher, Y.; Stangassinger, M.; Jain, R. K. Oncotic Pressure in Solid Tumors Is Elevated. *Cancer Res.* **2000**, *60*, 4251–4255.
23. Kim, S.; Shi, Y.; Kim, J. Y.; Park, K.; Cheng, J. X. Overcoming the Barriers in Micellar Drug Delivery: Loading Efficiency, *in Vivo* Stability, and Micelle–Cell Interaction. *Expert Opin. Drug Deliv.* **2010**, *7*, 49–62.
24. Matsumura, Y. Polymeric Micellar Delivery Systems in Oncology. *Jpn. J. Clin. Oncol.* **2008**, *38*, 793–802.
25. Shin, H. C.; Alani, A. W.; Rao, D. A.; Rockich, N. C.; Kwon, G. S. Multi-Drug Loaded Polymeric Micelles for Simultaneous Delivery of Poorly Soluble Anticancer Drugs. *J. Controlled Release* **2009**, *140*, 294–300.
26. Kim, S. C.; Kim, D. W.; Shim, Y. H.; Bang, J. S.; Oh, H. S.; Wan Kim, S.; Seo, M. H. *In Vivo* Evaluation of Polymeric Micellar Paclitaxel Formulation: Toxicity and Efficacy. *J. Controlled Release* **2001**, *72*, 191–202.
27. Kim, D. W.; Kim, S. Y.; Kim, H. K.; Kim, S. W.; Shin, S. W.; Kim, J. S.; Park, K.; Lee, M. Y.; Heo, D. S. Multicenter Phase II Trial of Genexol-PM, a Novel Cremophor-Free, Polymeric Micelle Formulation of Paclitaxel, with Cisplatin in Patients with Advanced Non-small-Cell Lung Cancer. *Ann. Oncol.* **2007**, *18*, 2009–2014.
28. Shin, H. C.; Alani, A. W.; Cho, H. A.; Bae, Y. S.; Kolesar, J. M.; Kwon, G. S. A 3-in-1 Polymeric Micelle Nanocontainer for Poorly Water-Soluble Drugs. *Mol. Pharm.* **2011**, *8*, 1257–1265.
29. Hoang, B.; Lee, H.; Reilly, R. M.; Allen, C. Noninvasive Monitoring of the Fate of ^{111}In-Labeled Block Copolymer Micelles by High Resolution and High Sensitivity Micro-SPECT/CT Imaging. *Mol. Pharm.* **2009**, *6*, 581–592.
30. Cho, H. A.; Indig, G. L.; Weighert, J.; Shin, H. C.; Kwon, G. S. *In Vivo* Cancer Imaging by Poly(ethylene glycol)-*b*-poly(ε-caprolactone) Micelles Containing a Near-Infrared Probe. *Nanomedicine* **2011**, 10.1016/j.nano.2011.06.009.